

## **General Disclaimer**

### **One or more of the Following Statements may affect this Document**

- This document has been reproduced from the best copy furnished by the organizational source. It is being released in the interest of making available as much information as possible.
- This document may contain data, which exceeds the sheet parameters. It was furnished in this condition by the organizational source and is the best copy available.
- This document may contain tone-on-tone or color graphs, charts and/or pictures, which have been reproduced in black and white.
- This document is paginated as submitted by the original source.
- Portions of this document are not fully legible due to the historical nature of some of the material. However, it is the best reproduction available from the original submission.

TEM OBSERVATIONS ON GRAIN BOUNDARIES IN SINTERED SILICON

Annual Report

Part 1

1 January 1977 - 30 September 1978

JPL Contract No. 954852

by

D. Ast and H. Föll

Prepared by

D. G. Ast

Materials Science and Engineering  
Bard Hall, Cornell University  
Ithaca, New York 14853

The JPL low-cost solar array project is sponsored by the U.S. Department of Energy and forms part of the Solar Photovoltaic Conversion Program to initiate a major effort toward the development of low-cost solar arrays. This work was performed for the Jet Propulsion Laboratory, California Institute of Technology by agreement between NASA and DOE.

### Introductionary remarks

The Material Science Department at Cornell University studies the structure and electronic properties of grain boundaries in Si with a two-fold approach.

The first approach is to analyse grain boundaries as they occur in polycrystalline Si specimens, especially those prepared by EFG, with a combination of optical microscopy, Ebic, and Tem.

The second approach is to prepare bicrystals which contain one grain boundary of a predetermined geometry. Although less related to practical problems, this approach has the advantage that variations in the boundary structure can systematically be investigated as a function of the orientation between the two crystals.

This report presents the results obtained to day, using the latter approach. Feedback by other contractors to JPL as to where the methods used here (such as high resolution multi-beam imaging) might be useful in solving applied problems is requested.

D.G.Ast

# TEM OBSERVATIONS ON GRAIN BOUNDARIES IN SINTERED SILICON

H. Föll<sup>1)</sup> and D. Ast

Department of Materials Science and Engineering,  
Cornell University, Ithaca, N.Y. 14853

## ABSTRACT

Grain boundaries in silicon with a predetermined orientation were prepared by the sintering of two single crystals. A combination of standard transmission electron microscopy and lattice imaging was used to investigate the structure of the boundaries produced. Low angle grain boundaries on {100} and {111} planes, and twin boundaries on {111} planes are discussed in detail.

1) Present address: IBM Research Center, P.O. Box 218, Yorktown Heights,  
New York 10598

## 1. INTRODUCTION

The structure and properties of grain boundaries in covalently bonded crystals such as silicon and germanium has been studied only to a limited degree in comparison to metals (cf., e.g., Chadwick and Smith 1976). The proposed use of polycrystalline silicon for solar cells has recently stimulated research in the structure and properties of grain boundaries in semiconductors with particular emphasize on their influence on device properties (see, e.g., Ravi and Wald 1977).

Grain boundaries may influence the performance of solar cells in several ways, e.g., by acting as recombination center for carriers decreasing the short circuit current or as shunts reducing the open circuit voltage. In addition, grain boundaries may cause local increases in the diffusion of dopants or interact with residual impurities. In general, the presence of grain boundaries is likely to decrease the efficiency of a solar cell.

On the other hand, grain boundaries can be used as active elements in a device and grain boundary transistors have been made (Mataré 1971); their principles of operation are however not fully understood.

The most interesting and presently unsettled question is whether the electronic properties of grain boundaries can be understood in terms of the primary and secondary dislocations which, accordingly to widely accepted grain boundary models (see, e.g., Bollmann 1970, Pumphrey 1972, Ralph, Howell and Page 1973), form the boundary.

Except for small-angle tilt boundaries (Bourret and Dessaux 1978) and a special  $\Sigma 9$  boundary (Krivanek, Isoda and Kobayashi 1977) the structure of grain boundaries in semiconductors has not been studied in detail. A preparation technique which allows to obtain specimens with a well defined boundary geometry greatly facilitates an investigation of grain boundaries. In silicon, the most promising technique seemed to be the sintering of two single crystals similar to the method first introduced for Au thin films by Schober and Balluffi (1970). This paper demonstrates the feasibility of the sintering method and analyses some of the boundaries obtained. Transmission electron microscopy (TEM) was used to characterize the boundaries. Extensive use was made of the weak-beam technique (Cockayne, Ray and Whelan 1969) and of lattice imaging. It appears that silicon is an especially suitable material for general research of grain boundary structures and that high resolution techniques are capable of extending the limits of conventional TEM to dimensions in the nm region.

## 2. EXPERIMENTAL

Silicon in air is always covered with a  $\text{SiO}_2$  layer a few nanometers thick. The presence of this layer presumably prevents sintering when one crystal is placed on top of the other one without pressure, even at temperatures close to the melting point (K. Mayer, priv. com.) This interpretation is supported by the observation that Si wafers in accidental contact during heat treatment in a reducing atmosphere tend to stick together (B. Kolbesen, priv. com.). We therefore started our sintering experiments in a hydrogen atmosphere using the experimental set-up shown in Fig. 1. Critical parameters for sintering are the temperature  $T$ , the pressure on the samples  $p$ , the sintering atmosphere, and the surface conditions of the samples. The conditions sufficient for sintering are not fully understood at present; it appears that a pressure high enough to induce some plastic flow is essential. Sintered samples can be obtained, e.g., in a  $\text{H}_2$  atmosphere at  $T \sim 1200$  °C and  $p \sim 1$  Mpa using specimens with optically flat surfaces.

The silicon used was n - type cut from dislocation-free crystals grown by the float zone technique. Both surfaces of the wafer to be sintered were "Syton" polished to a mirror finish. The desired orientation relationship between the specimens was established by first cutting them along the required direction (as established by X-ray Laue diffractograms) and by subsequently aligning them along a flat in the graphite holder. Typically, a stack of up to twenty  $0.25 \times 5 \times 5$  mm samples were sintered together in one experiment.

After sintering, the specimen was cut either at  $90^\circ$  (for viewing the boundary end-on) or at  $25^\circ$  (for viewing the boundary flat-on after tilting in the TEM) with respect to the boundary plane. The resulting specimens were then either chemically thinned or ion-milled. A Siemens Elmiskop 102 was used for observation, usually operated at 125 kV and at instrument magnifications of typically 100 000x, 200 000x or 800 000x.

## 3. RESULTS AND DISCUSSION

### 3.1 General Observations

Although usually all Si slices adhered together, sintering did not always occur over the whole area of the sample. Deformation induced dislocations, mostly

arranged in bundles or subboundaries, were frequently observed. In contrast to sintered Au crystals (Scober and Balluffi 1970) hardly any gas bubbles were formed in the boundary. Instead, unidentified amorphous regions appeared in or close to the boundary. Fig. 2 gives an impression of the over-all appearance of a sintered boundary, the amorphous regions are clearly visible. Fig. 3 resulted when lattice imaging techniques were applied in order to confirm the amorphous structure of this regions. It is tempting to assume that this amorphous regions are remainders of the original oxide layer on the sample, but so far this could not be proved.

### 3.2. Twist Boundaries on {100} Planes

Low-angle ( $\Sigma = 1$ , with misorientations up to  $8^\circ$ ) and, to a limited degree,  $\Sigma 5$  boundaries ( $\Sigma = 5$ , rotation angle  $\alpha \sim 37^\circ$ ) have been made by sintering. The  $\Sigma 5$  boundaries investigated did not show a secondary dislocation network although at the misorientations from the precise  $\Sigma 5$  orientation investigated ( $\sim 1.5^\circ$ ) the expected network spacing should have been large enough ( $\sim 7$  nm) to be safely detected. That a boundary was indeed formed during sintering was indicated by the presence of a parallel array of dislocations with rather large spacings (45 nm) which accommodated a small additional tilt component of the boundary. The reason for the absence of the expected network are not understood.

The low-angle twist boundaries exhibited the square network of screw dislocations expected from theory (Bollmann 1970). Fig. 4 shows a typical boundary with a dislocation spacing of  $\sim 9$  nm, corresponding to a misorientation of  $\sim 2^\circ$ , imaged under different diffraction conditions. Fig. 4d was obtained under multi-beam imaging conditions with the electron beam close to the  $\langle 100 \rangle$  direction; see the inset in Fig. 4d. This resulted in a very narrow contrast width of the dislocations ( $\sim 1.5$  nm) and shows all dislocations simultaneously. By comparing Fig. 4d with Fig 4a-c it can be seen that the multibeam image gives the best representation of the actual boundary structure. Furthermore, in contrast to weak-beam images it still gives good contrast in relatively thick specimen areas.

The screw dislocations forming the boundary are not visibly extended. This is in agreement with the observation of Packeiser and Haasen (1977) that a critical distance of  $\sim 100$  nm exists, well above the network spacing, before a dislocation emerging from a dislocation node reaches its equilibrium dissociation width.

The most remarkable feature of the network (besides its regularity) are the frequent displacements of the network. This displacement usually is about one-half

of the network spacing and runs along irregularly curved lines. Schober and Balluffi (1971) observed similar phenomena in sintered Au bicrystals and identified these defects as "extraneous" dislocations, which they later called "extrinsic" dislocations (Balluffi, Komen and Schober 1972); the term "foreign" dislocations is also used (Bollmann 1970). These dislocations are thought to originate from the interaction of the screw dislocation network with lattice dislocations (= extrinsic dislocations). The structure of extrinsic dislocations in the boundary according to Schober and Balluffi (1971) is shown in Fig. 5a. These authors could not directly confirm the proposed structure since the spacing of their networks was too small. The silicon boundaries give a better idea of the actual structure (cf. Fig. 6) but details are still not fully revealed.

Extrinsic dislocations introduce tilt components in the boundary. Formally, this can be described by attributing to them an "effective" Burgers vector, representing only the Burgers vector component perpendicular to the boundary (Schober and Balluffi 1971). These authors also showed that this effective Burgers vector can account for most of the contrast behaviour of an extrinsic dislocation at small network spacings.

Fig. 7 shows a low-angle boundary on {100} with roughly equal twist and tilt components ( $\sim 1.8^\circ$ ). In this case the spacing between the extrinsic dislocations is about the same as that of the screw dislocations ( $\sim 1.2$  nm). It can be seen that the extrinsic dislocations partially substitute for the original screw dislocations; the distance between the pure screw dislocations parallel to the extrinsic dislocations (Fig. 7a) is about twice the spacing of the screw dislocations perpendicular to the latter.

When the dislocation reaction between the screw dislocation network and a lattice dislocation involves glide processes only, the resulting extrinsic dislocation is necessarily associated with a step in the boundary plane, cf. Fig. 5b. In this case all dislocations must lie in their {111} glide planes and the step height in the {100} boundary plane is  $\sim 0.7 d$  ( $d$  = network spacing)

From this consideration one sees that extrinsic dislocations may be formed for a variety of reasons:

- i) in order to compensate tilt components in the boundary
- ii) in order to accommodate steps in the boundary
- iii) in order to allow faceting, e.g., if the sintered surfaces are not exactly {100} planes the boundary very likely will form facets on {100}.
- iv) in order to absorb (or to emit) a lattice dislocation

In the first three cases extrinsic dislocations, contrary to the implication

of their name, are an equilibrium part of the grain boundary.

The spacing of the network dislocations decreases with increasing misorientation and the boundary structure becomes more and more difficult to observe. Fig. 8 shows a network with a spacing of 2.7 nm taken with the multibeam conditions mentioned above. The contrast is very low and the interpretation of the micrograph is difficult since part of the contrast arises from the interference of the various extra diffraction spots produced by the grain boundary (Sass, Tan and Balluffi 1975). In fact, the spacing of the fringes is only one-half of what one would expect for dislocations, knowing the misorientation angle of the boundary from the diffraction pattern. This proves that the observed structure is due to Moiré effects between diffracted  $\{200\}$  beams. In this case it is easier to obtain information on the boundary by an analysis of the diffraction pattern (Carter, Donald and Sass 1973) or by utilizing lattice imaging techniques. Diffraction effects require a more extended discussion and are subjected to a forthcoming paper. An example of the application of lattice imaging is given in Fig. 9 which shows  $\{111\}$  lattice fringes across two low-angle twist boundaries on  $\{100\}$ . One set of the screw dislocations forming the boundary is clearly visible by the shift of the fringes along the dislocation lines; for a detailed discussion of the contrast of screw dislocations see Cockayne, Parsons and Hoelke (1971). The spacing between the dislocations is 2.7 nm (Fig. 9a) and 6.5 nm (Fig. 9b), respectively. Fig. 9a shows the boundary of Fig. 8 and demonstrates clearly that the boundary structure is scaled down but otherwise similar to the structure at larger spacings; information not easily obtainable with standard TEM methods.

It appears that these micrographs may allow a direct measurement of the core size of the dislocations. This may however not be the case since contrast theories are not yet developed enough to account for details of the contrast in this particular imaging mode. Contrast artifacts such as, e.g., Moiré effects, are possible and cannot be ruled out without further work.

### 3.3. Twist Boundaries on $\{111\}$ Planes

Two systems have been investigated in detail: The  $\Sigma 1$  low-angle twist boundary (Füßl and Ast 1978) and the  $\Sigma 3$  twin boundary ( $\alpha = 60^\circ$ ). A hexagonal network of screw dislocations is expected with Burgers vectors  $\underline{b} = a/2\langle 110 \rangle$  for the  $\Sigma 1$  boundary and  $\underline{b} = a/6\langle 112 \rangle$  for the  $\Sigma 3$  boundary.

Fig. 10 shows the dislocation network observed in a  $\Sigma 1$  boundary for a very small misorientation ( $\alpha \sim 0.5^\circ$ ). The dislocation nodes are extended and overlap

thus forming a "node network" of dislocation nodes with alternately intrinsic and extrinsic stacking faults.

At amorphous regions the network often terminates by forming stacking-fault double ribbons which have been used to obtain an accurate value of the ratio of the intrinsic to extrinsic fault energy as well as the absolute values. (Föll and Carter 1978).

At smaller dislocation spacings conventional TEM again ceases to give very useful information and it becomes advantageous to resort to lattice imaging. Fig. 11 contrasts a conventional weak-beam image, much obscured by Moiré effects, with a lattice fringe image of the same boundary (Fig. 11b). The lattice fringe picture clearly shows localized bending of the fringes indicating the presence of dislocations in the boundary and in some cases lattice fringe images were actually able to prove the existence of dislocations when standard imaging techniques failed to do so. A schematic outline of the node network, down-scaled to the proper size from the observed configuration of Fig. 10 is included in Fig. 11. It can be seen that the shift of the lattice planes by the dislocations running inclined to the fringes apparently is too small to be clearly visible; these dislocations should be visible by using a different set of  $\{111\}$  fringes. This is indeed the case as demonstrated in Fig. 12. The dislocation lines appear to be straighter than expected from the node model; this may indicate that the extrinsic nodes are constricted below a certain spacing of the dislocations and that a triangular network is formed.

Fig. 13 shows the dislocation networks in boundaries close to a twin orientation. The network spacing is about 10 nm and 4.5 nm corresponding to a deviation from the exact  $\Sigma 3$  orientation of  $\approx 1.3^\circ$  and  $2.8^\circ$ , respectively. Contrast analysis proved that the networks consist of a hexagonal array of screw dislocations with a Burgers vector  $\underline{b} = a/6\langle 112 \rangle$ , the base vector of the DSC lattice related to a  $\Sigma 3$  boundary. Similar networks in twin boundaries have been observed in Au by Erlings and Schapinsky (1978).

### 3.4 Additional Observations

Direct lattice images of twist boundaries with the boundary end-on and the specimen in a  $\langle 110 \rangle$  orientation can also be obtained; Fig. 14 shows examples. Simultaneous imaging of both sides of the boundary, although in different crystallographic orientation, is possible because the crystal lattice is basically undisturbed across the boundary (apart from elastic distortions); all necessary misfit is concentrated in the dislocations. Alignment of the electron beam

exactly parallel to the  $\langle 110 \rangle$  axis on the boundary with the aid of the diffraction pattern is difficult in practice because the diffraction pattern originates mainly from areas far away from the boundary and thus shows two  $\{110\}$  poles, the center of which should correspond to the  $\{110\}$  pole on the boundary. Alignment of this center with the optical axis of the microscope has to be done by trial and error. The resulting uncertainties of the imaging conditions prohibit a quantitative interpretation of the images obtained in terms of atom positions (cf. Spence, O'Keefe and Kolar 1977, Dessaux, Renault and Bourret 1977). Even if the imaging conditions were perfectly known, however, such an analysis could only be carried out for the very restricted class of defects which are precisely aligned with  $\langle 110 \rangle$ , such as the dislocations in a pure tilt boundary (cf. Krivanek et al. 1977, Bourret and Dessaux 1978).

Despite this restriction the micrographs still contain useful informations: The  $\{111\}$  lattice fringes parallel to the boundaries are undisturbed, indicating the absence of any significant tilt component and perfect sintering. Stacking faults, both intrinsic and extrinsic are clearly visible and so are terminating fringes, indicating the presence of dislocations. Thus, as in the case of the lattice fringe images discussed earlier, these images confirm that a network of primary dislocations is still present at spacings of  $\sim 3$  nm. In addition, the presence of stacking faults indicates the existence of extended dislocation nodes even at this small spacings.

Fig. 14b shows a semicoherent and several fully coherent precipitates in addition to the boundary. Both types of precipitates give rise to intensity modulations of the fringes. Assuming that the lattice parameter of the precipitates is slightly different from the Si matrix this can be understood as a Moiré effect. In addition to the Moiré contrast, interface dislocations are visible in the semicoherent precipitate.

Fig. 15 shows a weak beam image of a low-angle boundary on a  $\{111\}$  plane. The boundary shows the appropriate contrast in the left-handed area; the appearance of the right hand side however is that of a twin boundary. Similarly, patches of dislocation network with a low-angle boundary structure are frequently observed in twin boundaries. These observations suggest that a low-angle boundary may split into two twin boundaries (i.e a microtwin) and the misfit dislocation network, which can be located either in the plane of one of the twin boundaries or in the perfect crystal. In the first case a twin-like hexagonal network would be formed, and in the second case a node network. Fig. 16 shows a lattice image containing both configurations: the dislocations change position from the middle of the micro-

twin to one of the twin boundaries. Besides the twist component the boundary in Fig. 16 contains a tilt component of  $5^\circ$  which was introduced by the emission of a small-angle tilt boundary about 200 nm away from the center of Fig. 16. Correspondingly, a near-twin boundary can "punch out" its dislocation network and thus split into a fully coherent twin boundary and a low-angle grain boundary.

#### 4. FINAL REMARKS AND CONCLUSIONS

Sintering of silicon single crystals was used successfully to prepare grain boundaries with a predetermined orientation. Optimization of the sintering process by a systematic variation of the sintering parameters is in progress. It is hoped that these studies will eventually lead to a deeper understanding of the sintering process itself and to the elimination of sintering artifacts such as precipitates. So far no attempts have been made to sinter specimens under very clean (semiconductor) conditions. With the present equipment, incorporation of impurities and a subsequent decoration of the boundary can be expected and precipitates have indeed been observed. For this reason the electrical properties of the boundaries have not yet been studied.

The grain boundaries obtained by sintering of Si samples proved to be well suited to investigate general properties of grain boundaries since silicon offers an unique combination of attractive properties:

- i) large dislocation-free crystals with high-quality surfaces (optically flat) of any desired orientation can be easily prepared, allowing the production of any boundary geometry.
- ii) A fairly large lattice constant (0.357 nm) provides relatively easy access to lattice imaging techniques with standard high-resolution microscopes and extends the range of TEM into atomic dimensions.
- iii) the immobility of dislocations in Si below  $700^\circ\text{C}$  (Alexander and Haasen 1968) conserves the boundary structure during all stages of specimen preparation and no artifacts due to thin-foil effects have been encountered.
- iv) The high Peierls force in Si tends to conserve the regularity of the network which is formed at high temperatures. For this reason thermal stresses during cooling have less effect on the regularity of the network than in metals and even networks with fairly large spacings tend to be very regular.

ACKNOWLEDGEMENTS

Many stimulating discussions with Dr. C.B. Carter are gratefully acknowledged. Thanks are due to Dr. B. Kolbesen from the Siemens AG Germany who provided the Si crystals for the experiments. This work was funded by DOE under contract No. EY-76-S-02-2894. Additional support in terms of facilities was received from the Materials Science Center at Cornell.

FIGURE CAPTIONS

Fig. 1 Schematic drawing of the sintering equipment .

Fig. 2 Kinematical bright-field image of a low-angle twist boundary on a  $\{111\}$  plane. The diffraction vector in this and the forthcoming figures is indicated by an arrow; here it is  $g = \{111\}$ .

Fig. 3 Direct lattice image of an amorphous region. White "dots" can be thought to correspond to the open channels in a  $\langle 110 \rangle$  direction; the spacing of the fringes is 0.31 nm.

Fig. 4 Low-angle twist boundary on a  $\{100\}$  plane imaged with different diffraction conditions.  $g = \{220\}$  in 4a,c;  $g = \{224\}$  in 4b; 4d was taken with multi-beam conditions close to the  $\{100\}$  pole. The  $\{220\}$  Kikuchi bands, the major diffraction spots and the position of the aperture on the primary beam is indicated.

Fig. 5 a) Extrinsic dislocation along a  $\langle 110 \rangle$  direction according to Schober and Balluffi (1971). A possible set for the Burgers vectors may be  $b_1 = a/2 [110]$ ;  $b_2 = a/2 [1\bar{1}0]$ ;  $b_3 = a/2 [0\bar{1}1]$ ;  $b_4 = a/2 [10\bar{1}]$ .  
b) Step in the boundary associated with an extrinsic dislocation.

Fig. 6 Extrinsic dislocations in the dislocation network of a low-angle twist boundary on a  $\{100\}$  plane.

Fig. 7 Low-angle boundary on a  $\{100\}$  plane with comparable amounts of twist and tilt components.

a) Extrinsic dislocations and one set of the screw dislocations (parallel to  $g = \{220\}$  ) are visible.

b) Extrinsic dislocations and the second set of screw dislocations are visible.

Fig. 8 Image of a low-angle twist boundary on a  $\{100\}$  plane with a twist angle of  $8^\circ$  taken under multi-beam conditions.

Fig. 9  $\{111\}$  lattice fringes across two low-angle boundaries on  $\{100\}$  planes. Tilted beam illumination and a specimen orientation close to a  $\{112\}$  pole was used for this and the following lattice fringe images. The spacing between the fringes is 0.31 nm.

Fig. 10 Low-angle twist boundary on a  $\{111\}$  plane imaged with different diffraction vectors.  $\underline{g} = \{220\}$  in 10a,c;  $\underline{g} = \{111\}$  in 10b;  $\underline{g} = \{224\}$  in 10d. Fig. 10b shows contrast from the stacking faults in the intrinsic nodes (the extrinsic nodes would be in good contrast by reversing the sign of  $\underline{g}$ ).

Fig. 11 Weak-beam and lattice fringe image of a low-angle twist boundary on a  $\{111\}$  plane.

Fig. 12 Low-angle twist boundary on a  $\{111\}$  plane imaged with two different sets of  $\{111\}$  lattice fringes.

Fig. 13 Dislocation networks in boundaries on a  $\{111\}$  plane close to a twin orientation imaged with  $\underline{g} = \{220\}$ .

Fig. 14 Direct lattice image of low-angle twist boundaries on  $\{111\}$  planes viewed end-on along a  $\langle 110 \rangle$  direction.

Fig. 15 Low-angle twist boundary on a  $\{111\}$  plane imaged with  $\underline{g} = \{224\}$  exhibiting the structure of a twin boundary in the right-hand side.

Fig. 16 Direct lattice image of a low-angle twist boundary on a  $\{111\}$  plane with an additional tilt component split into twin boundaries.

REFERENCES

~~PROGRAMME - DEPT NOT FILMED~~

Alexander, H., and Haasen, P., 1968, Sol. State Phys., 22, 27

Balluffi, R.W., Komen, Y., and Schober, T., 1972, Surface Science, 31, 68

Bollmann, W., 1970, Crystal Defects and Crystalline Interfaces (Heidelberg, New York: Springer Verlag)

Bourret, A., and Dessaux, J., to be published

Carter, C.B., Donald, A.M., and Sass, S.L., 1978, Phil. Mag., in press

Chadwick, G.A., and Smith, D.A. (eds.), 1976, Grain Boundary Structure and Properties, (New York: Academic Press)

Cockayne, D.J.H., Ray, I.L.F., and Whelan, M.J., 1969, Phil. Mag., 20, 1226

Cockayne, D.J.H., Parsons, J.R., and Hoelke, C.W., 1971, Phil. Mag., 24, 139

Dessaux, J., Renault, A., and Bourret, A., 1977, Phil. Mag., 35, 357

Föll, H., and Carter, C.B., 1978, to be published

Föll, H., and Ast, D., 1978, Proc. 9th Int. Cong. Elect. Micr., Toronto, Vol 1, p. 428

Krivanek, O.L., Isoda, S., and Kobayashi, K., 1977, Phil. Mag., 36, 931

Mataré, H.F., 1971, Defect Electronics in Semiconductors, (New York: Wiley Interscience)

Packeiser, G., and Haasen, P., 1977, Phil. Mag., 35, 821

Pumphrey, P.H., 1972, Scripta Met., 6, 107

Ralph, B., Howell, P.R., and Page, T.F., 1973, Phys. Stat. Sol. (b), 55, 641

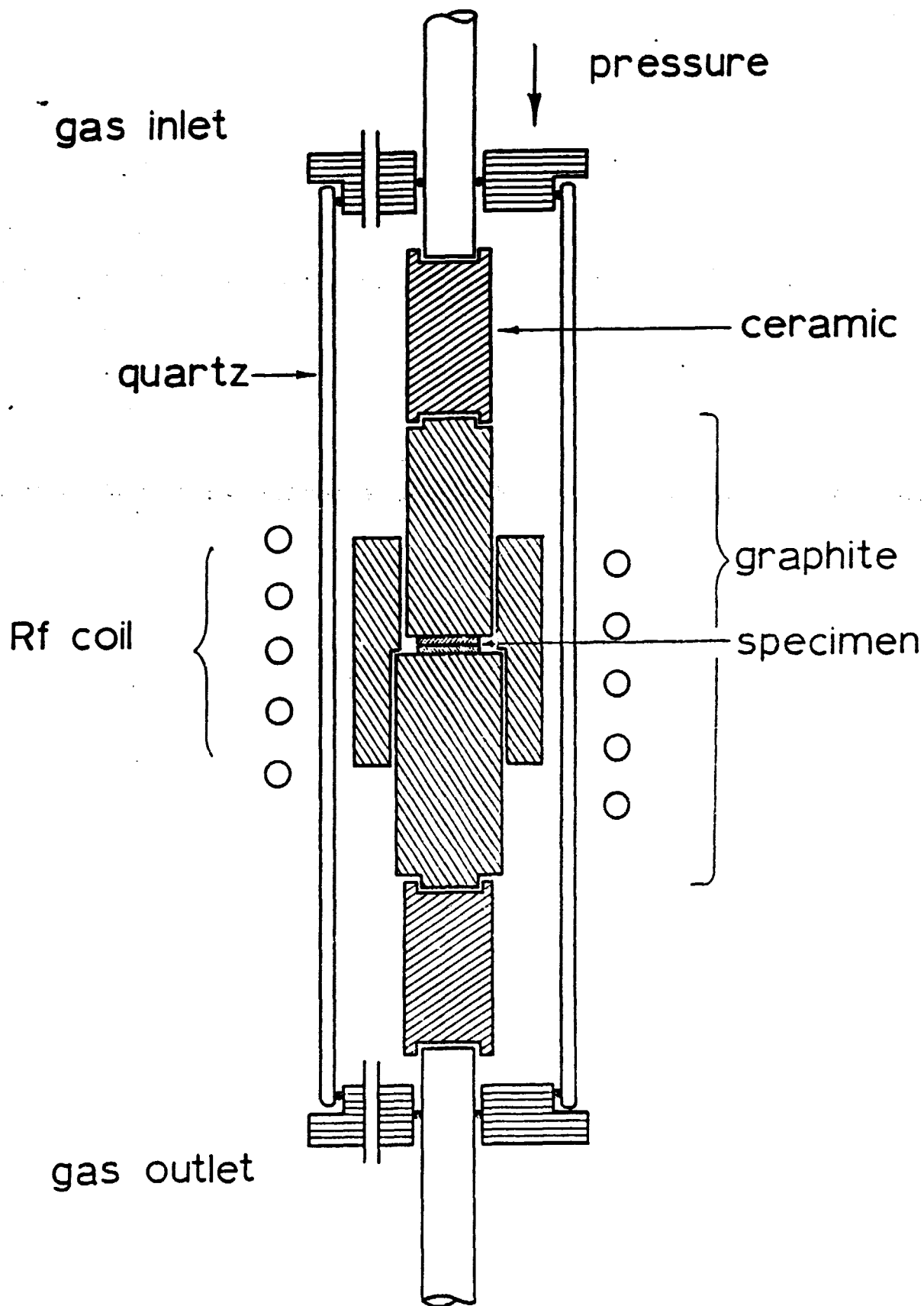
Ravi, K.V., and Wald, F.V., 1977, in: Semiconductor Silicon, edited by Huff, H.R. and Sirtl, E., (The Electrochemical Society), p. 820

Sass, S.L., Tan, T.Y., and Balluffi, R.W., 1975, Phil. Mag., 31, 559

Schober, I., and Balluffi, R.W., 1970, Phil. Mag., 21, 109

Schober, T., and Balluffi, R.W., 1971, Phil. Mag., 24, 165

Spence, J.C.H., o'Keefe, M.A., and Kolar, H., 1977, Optik, 49, 307



ORIGINAL PAGE IS  
OF POOR QUALITY

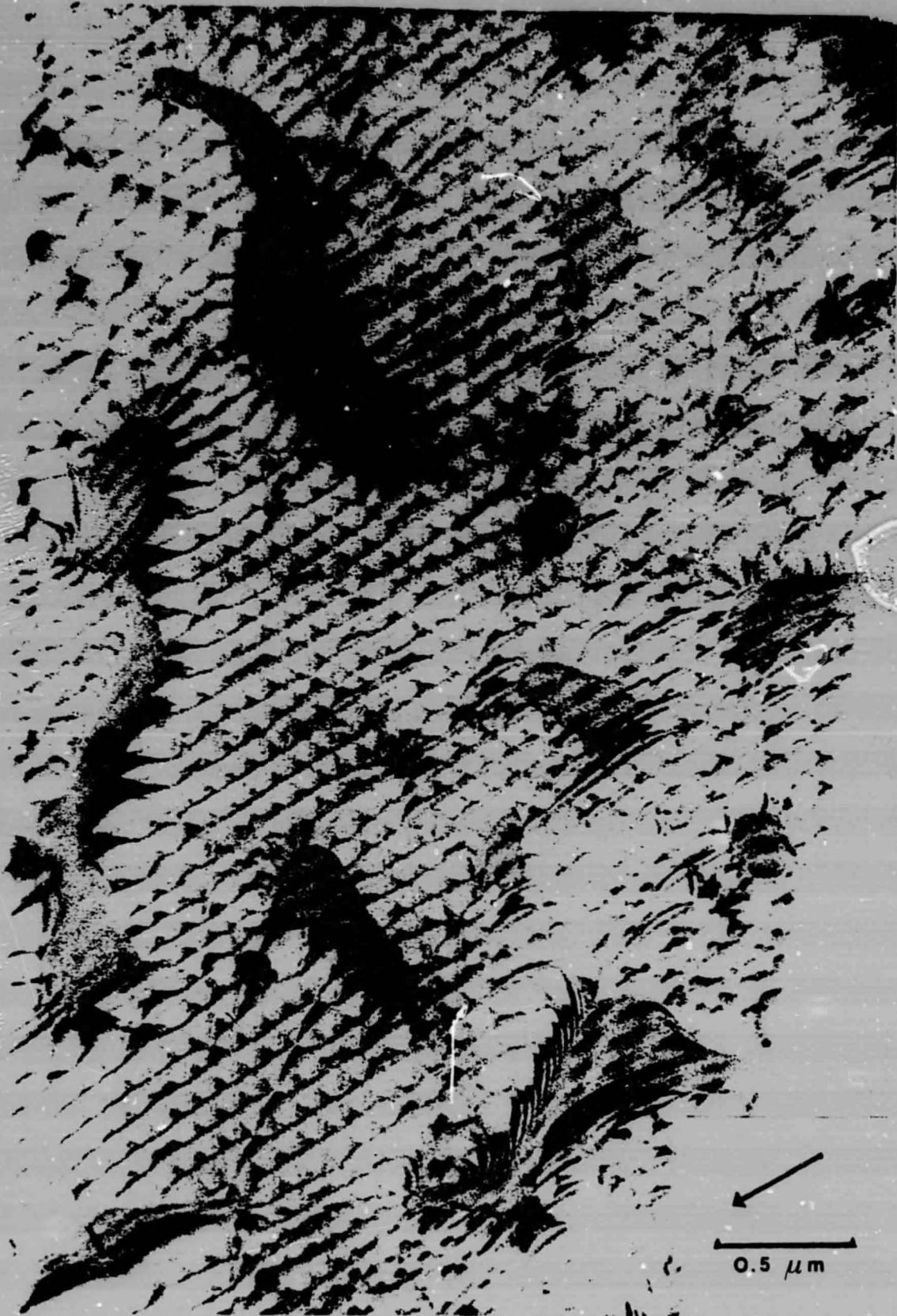


Fig. 2

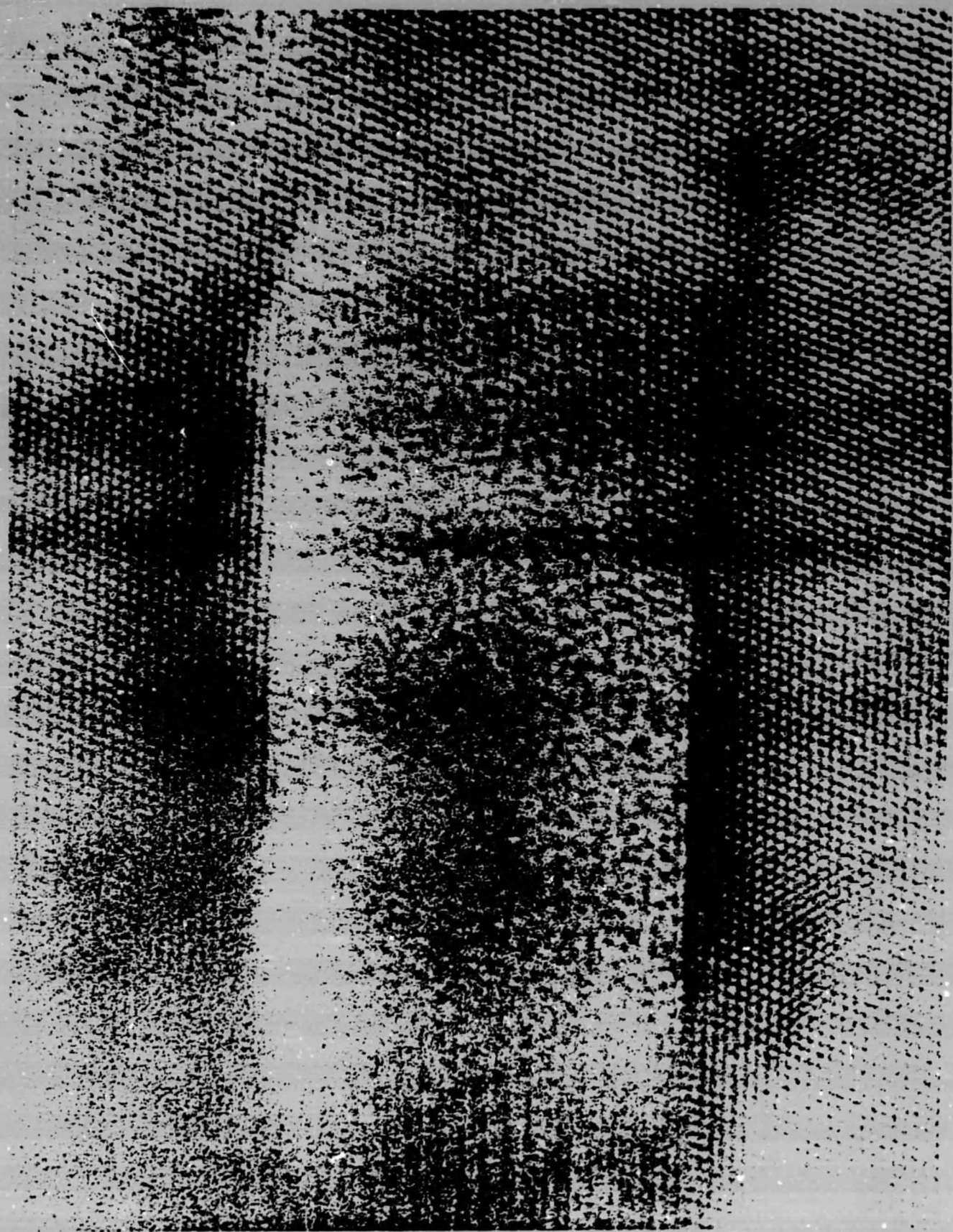
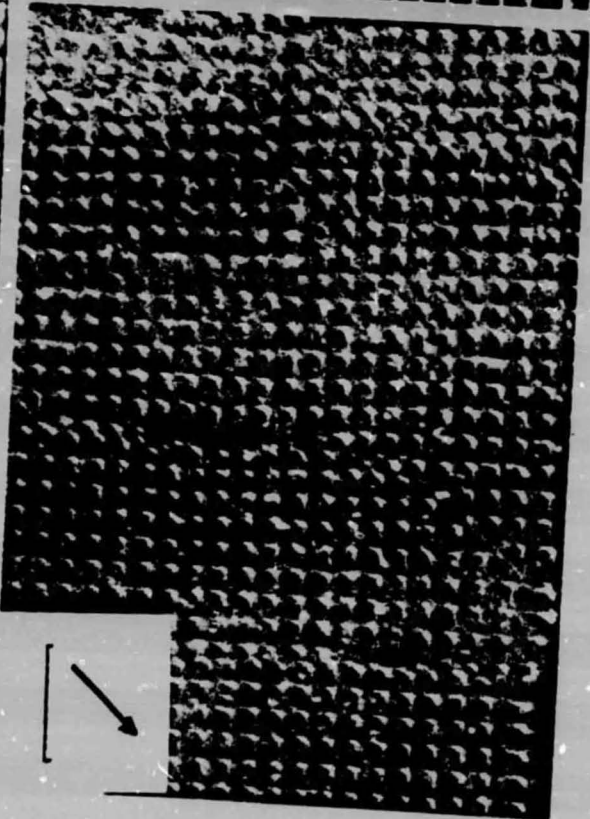
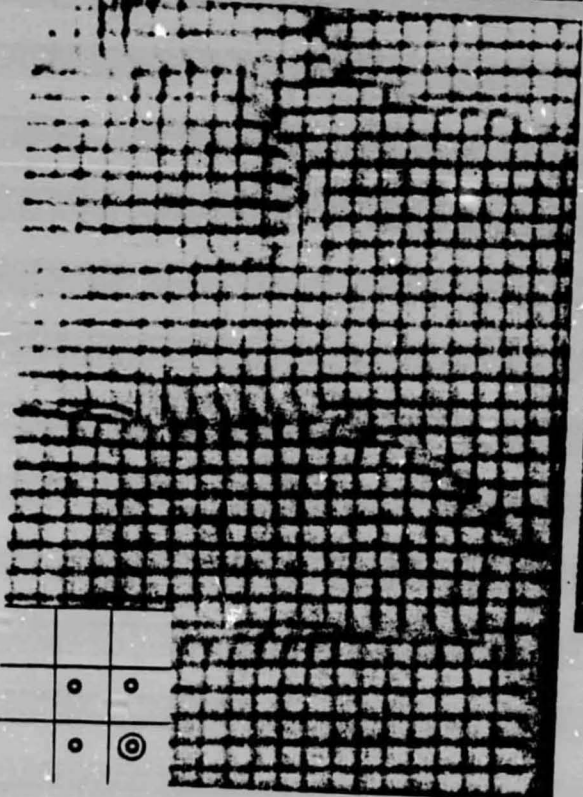
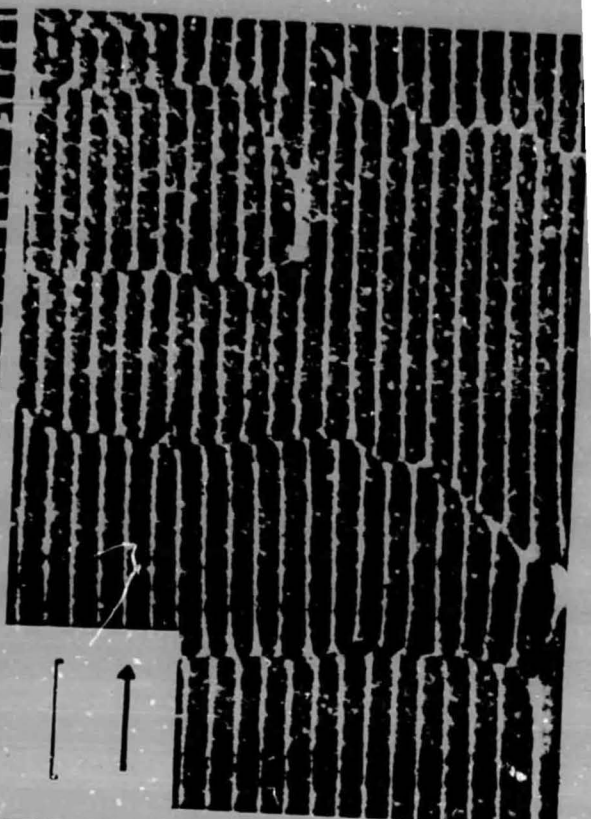
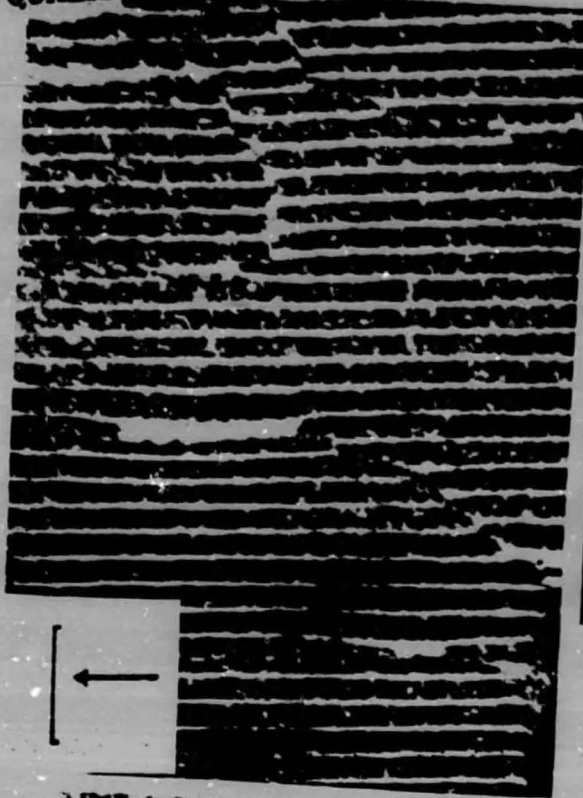
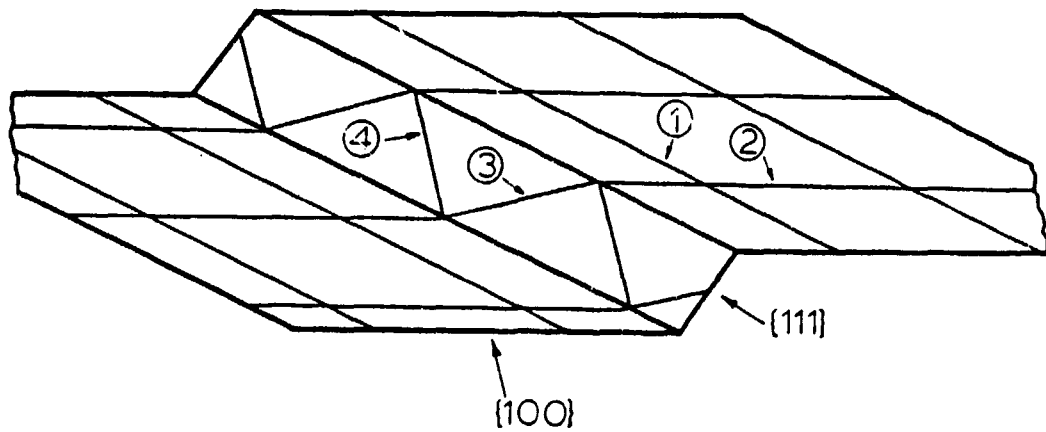
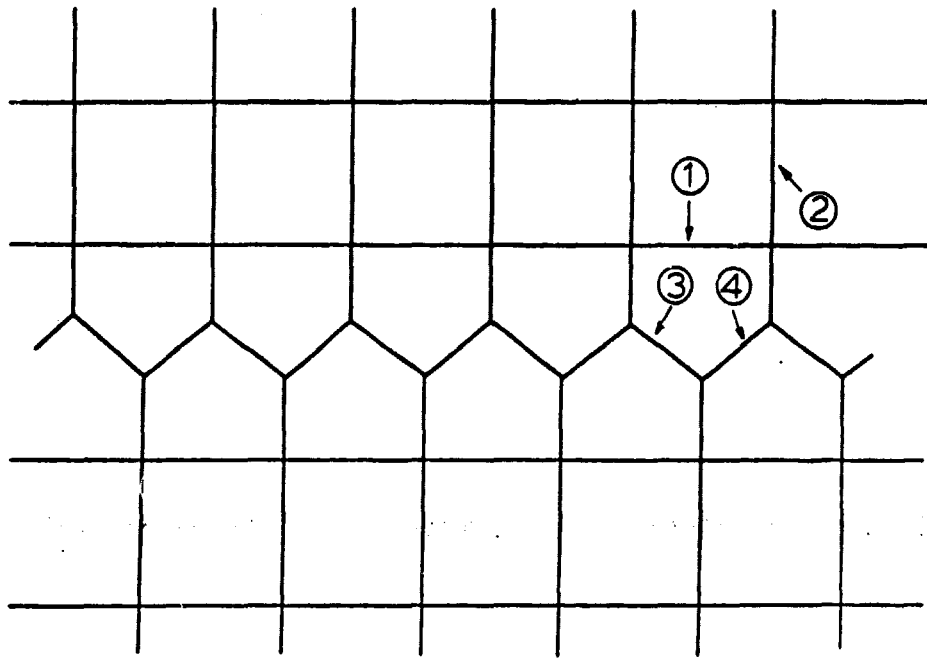


Fig. 3

ORIGINAL PAGE IS  
OF POOR QUALITY



	•	•
	•	⊙



ORIGINAL PAGE IS  
OF POOR QUALITY

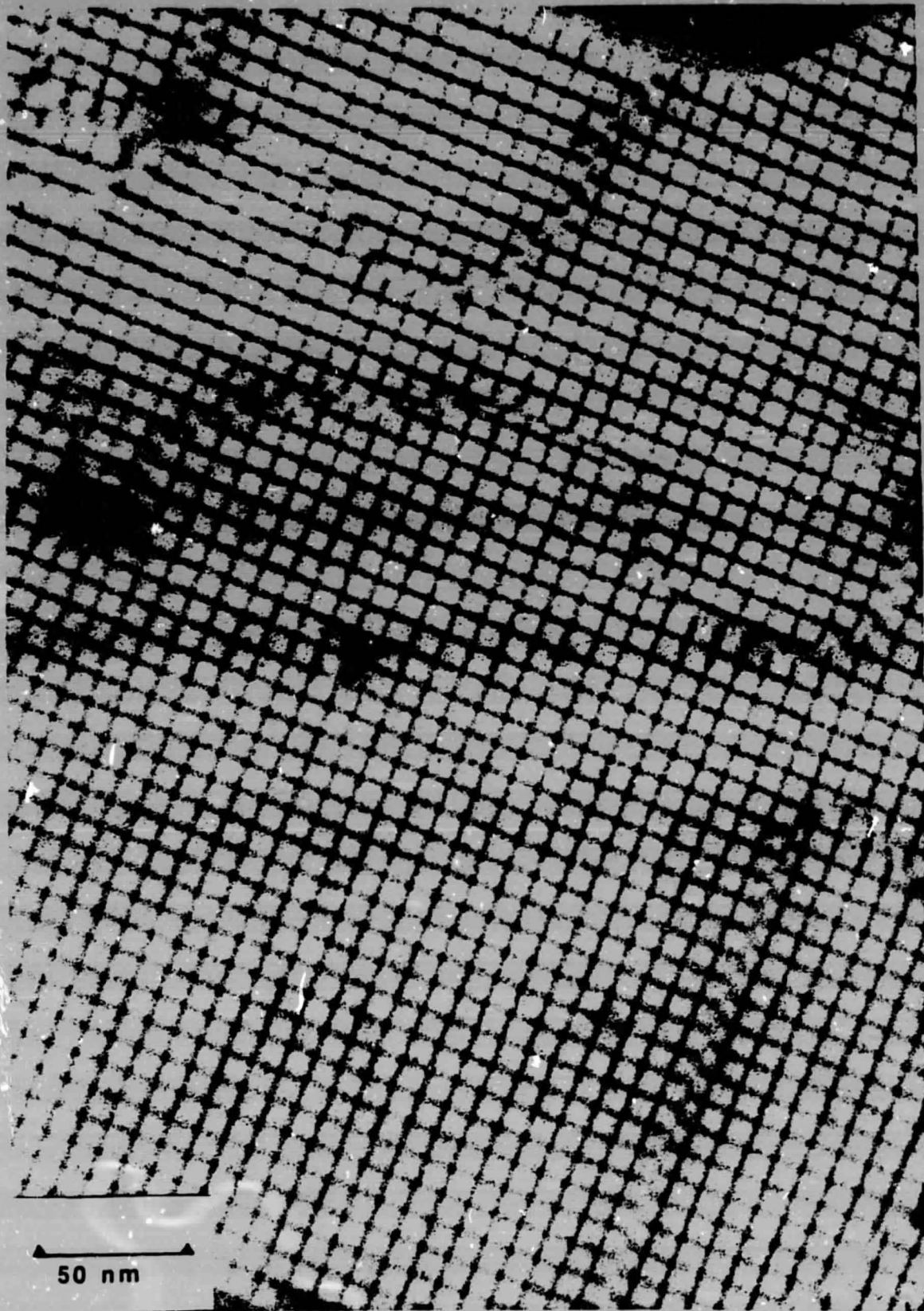
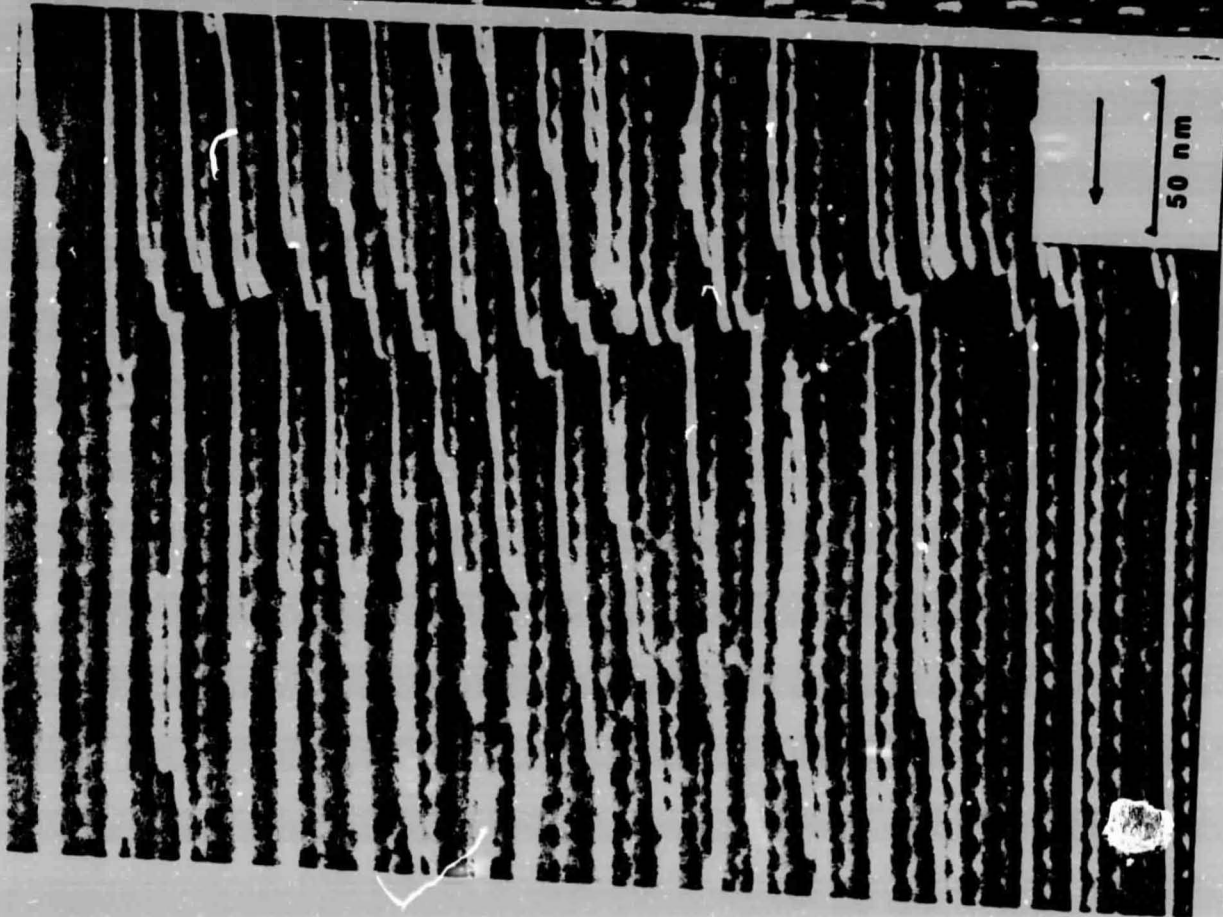
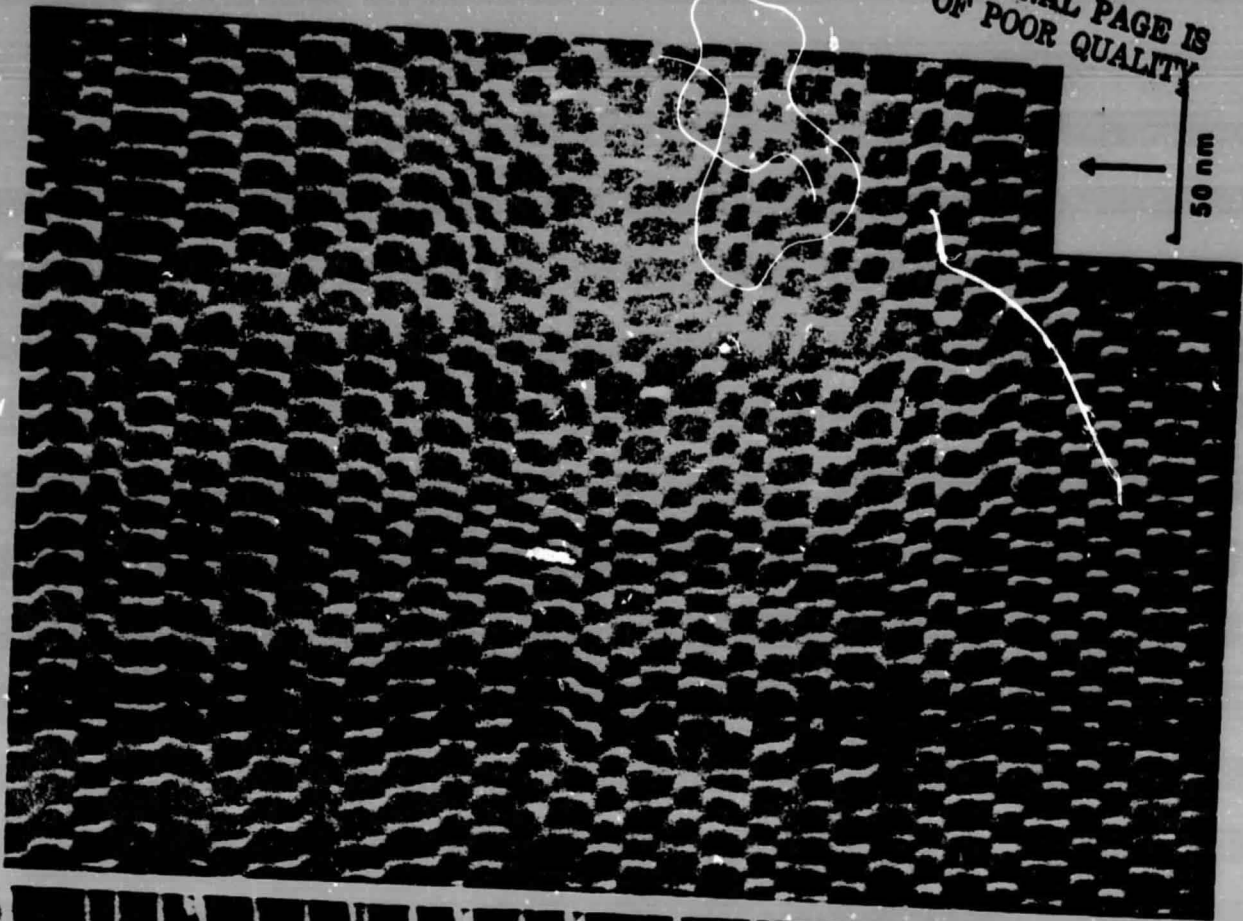


Fig. 6

ORIGINAL PAGE IS  
OF POOR QUALITY



ORIGINAL PAGE IS  
OF POOR QUALITY

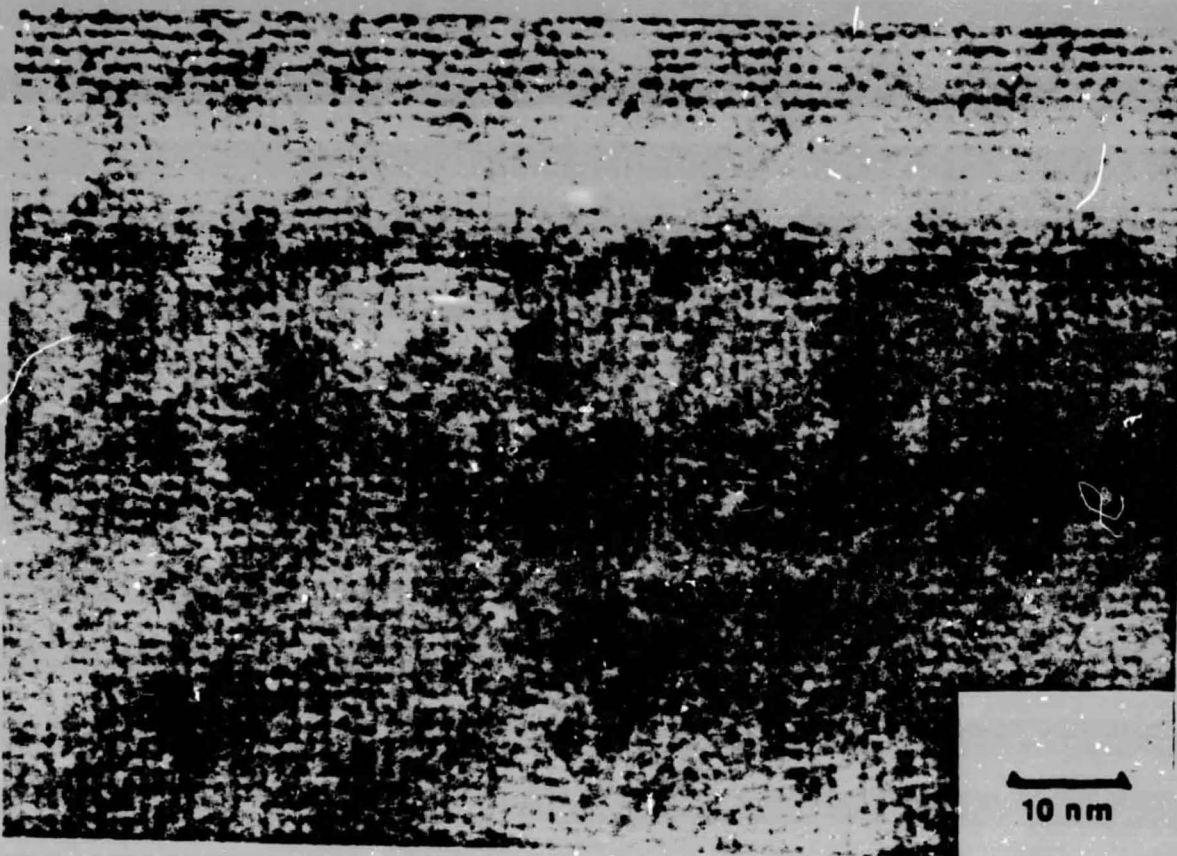
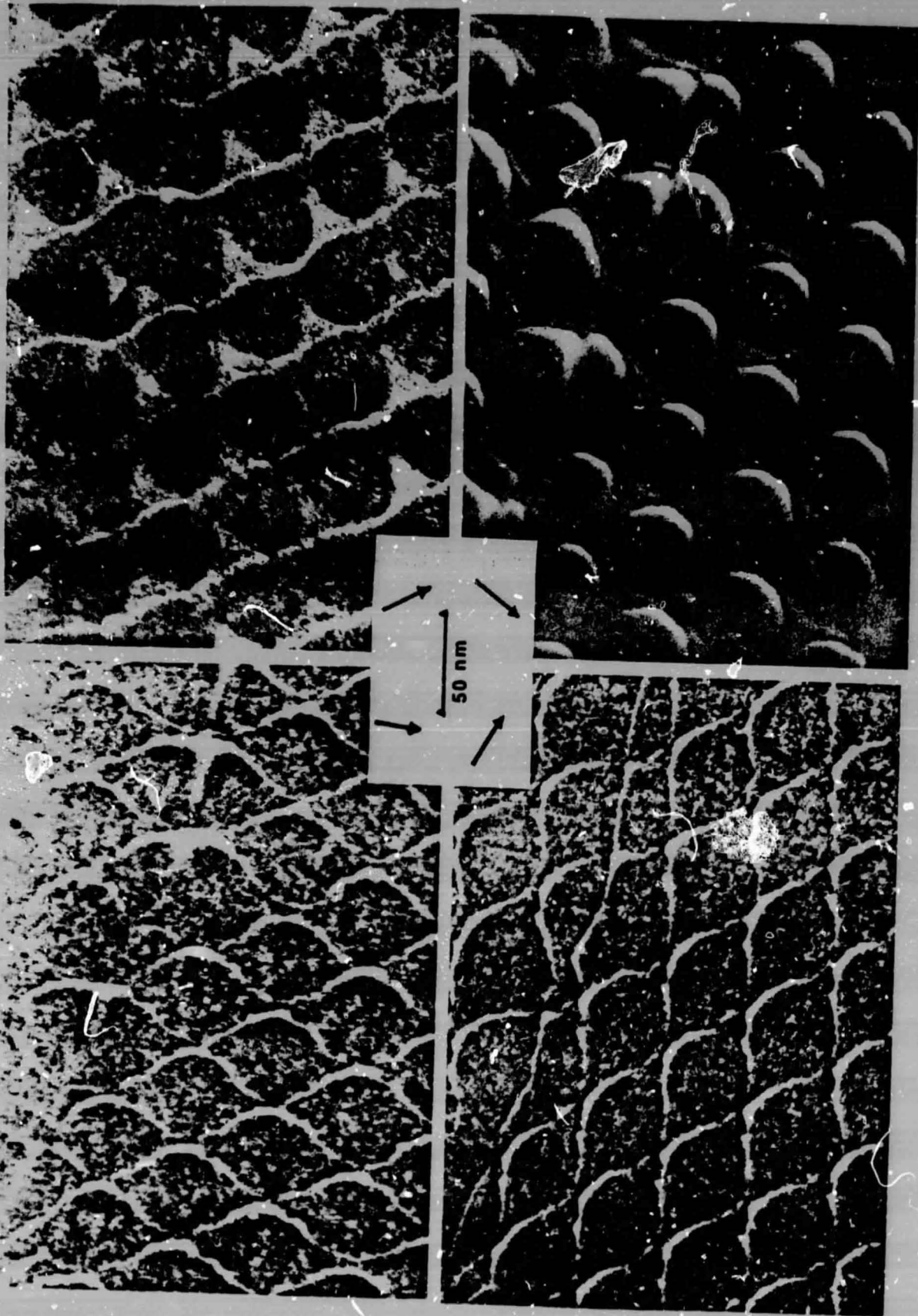
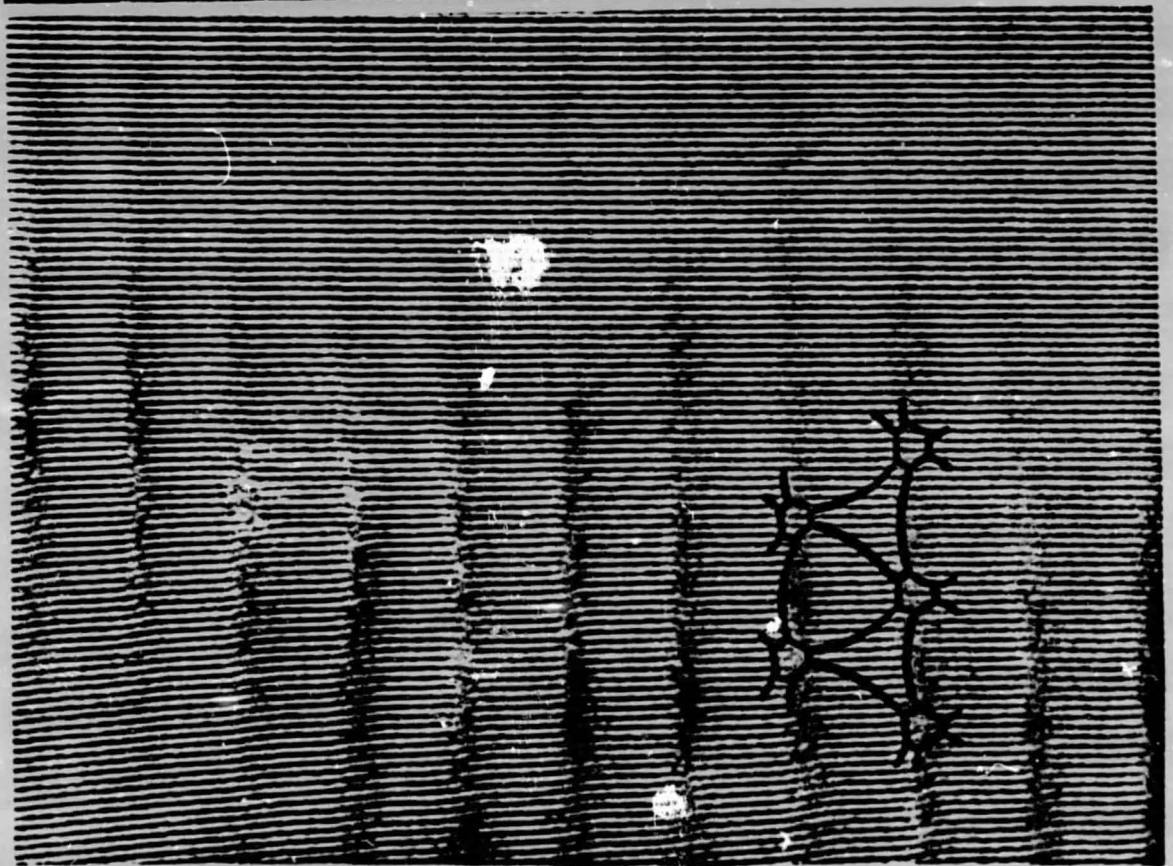
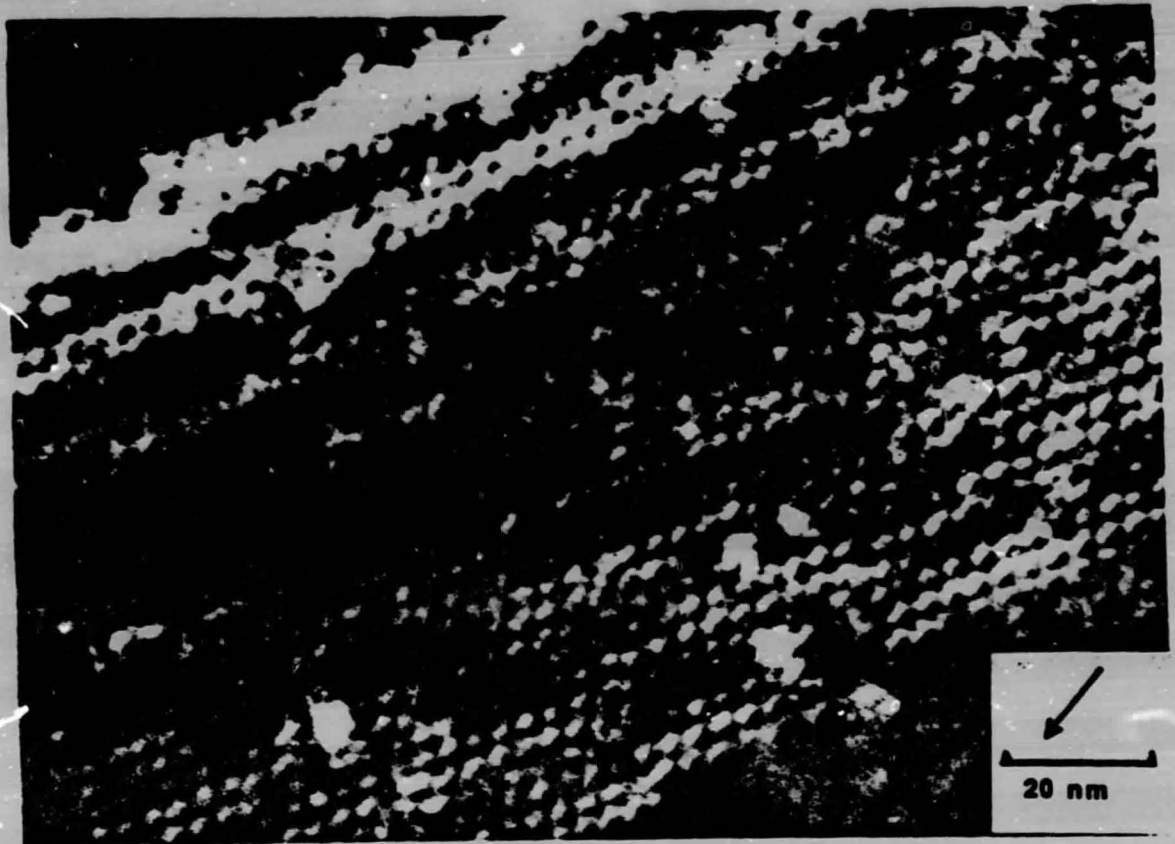


Fig. 8

ORIGINAL PAGE IS  
OF POOR QUALITY



ORIGINAL PAGE IS  
OF POOR QUALITY



ORIGINAL PAGE  
OF POOR QUALITY

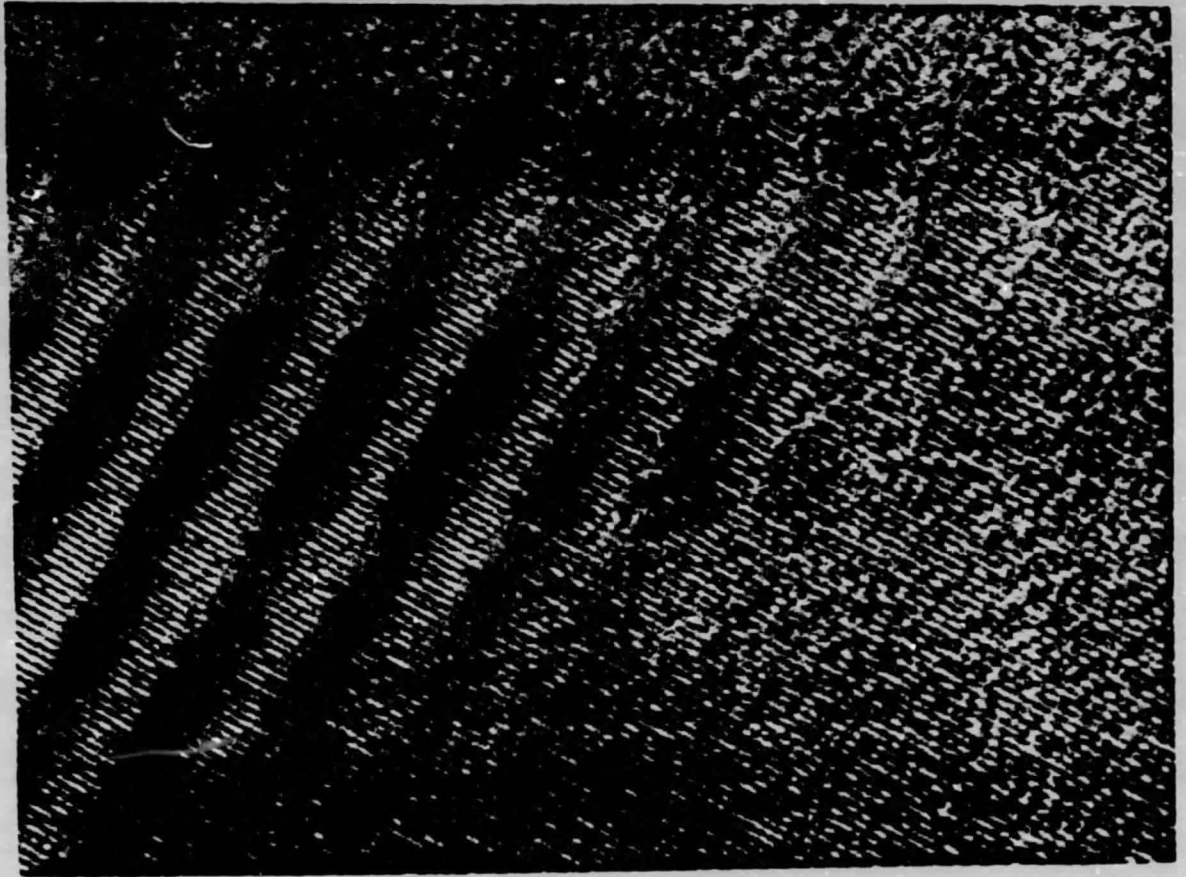
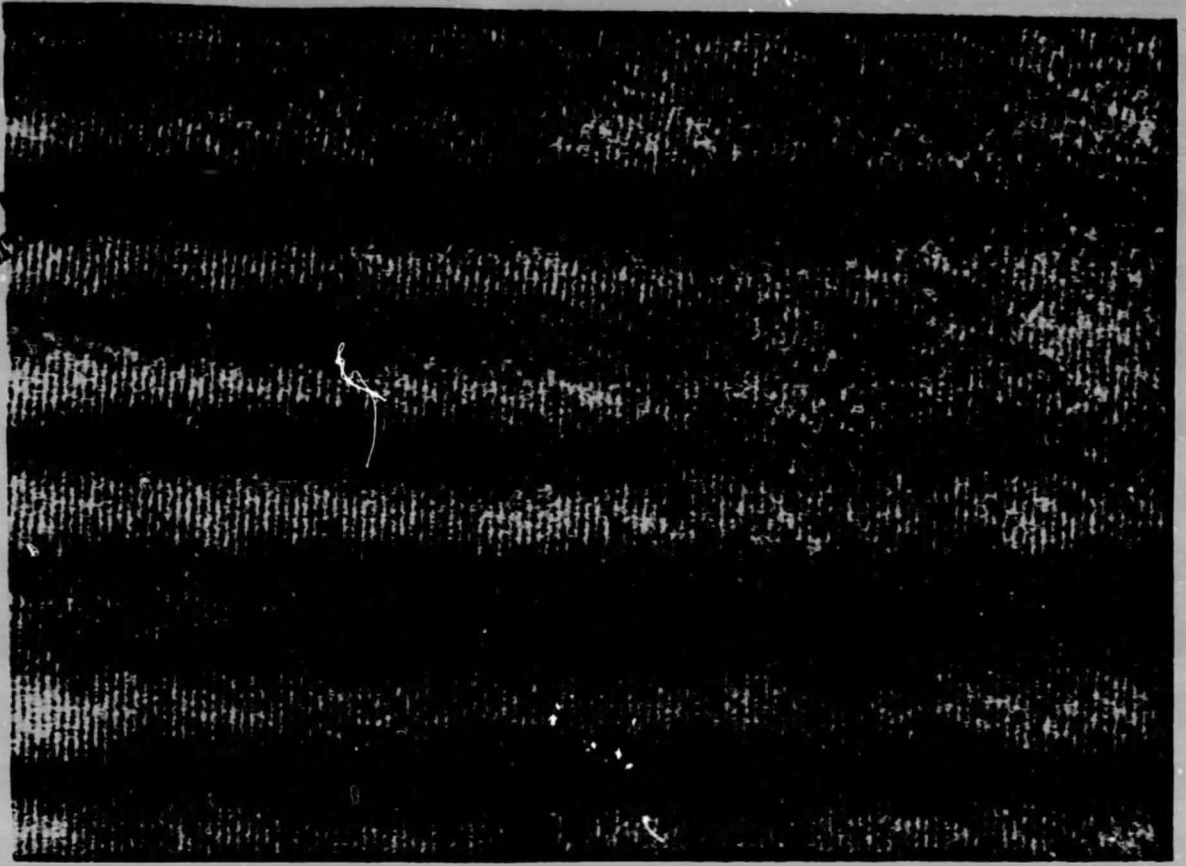


Fig. 17.

ORIGINAL PAGE IS  
OF POOR QUALITY

